LETTER • OPEN ACCESS

Study of the dependence of the magnetic moment of La$_{1-x}$Sr$_x$MnO$_3$ on the Sr doping level x

To cite this article: L. Q. Wu *et al* 2017 *EPL* **120** 27001

View the article online for updates and enhancements.

You may also like

Study of the dependence of the magnetic moment of La$_{1-x}$Sr$_x$MnO$_3$ on the Sr doping level x

L. Q. Wu[1,2], W. H. Qi[1], X. S. Ge[1], D. H. Ji[1], Z. Z. Li[1], G. D. Tang[1,3(a)] and W. Zhong[2]

[1] *Hebei Advanced Thin Film Laboratory, Department of Physics, Hebei Normal University
Shijiazhuang City, 050024, PRC*
[2] *Collaborative Innovation Center of Advanced Microstructures, National Laboratory of Solid State
Microstructures and Jiangsu Provincial Laboratory for Nanotechnology, Nanjing University
Nanjing, 210093, PRC*
[3] *State Key Laboratory of Magnetism, Institute of Physics, Chinese Academy of Sciences
Beijing 100190, PRC*

Abstract – The dependence of the magnetic moment of the perovskite manganites La$_{1-x}$Sr$_x$MnO$_3$ on the Sr doping level, x, is fitted using an oxygen $2p$ itinerant electron model for magnetic oxides (*i.e.*, the IEO model), which is similar to the O $2p$ hole model proposed by Alexandrov *et al.* (*Phys. Rev. Lett.*, **96** (2006) 117003). According to this IEO model, the itinerant electrons in these manganites are oxygen $2p$ electrons (or $2p$ holes) rather than $3d$ electrons, as assumed in the double-exchange interaction model. Furthermore, the proposed IEO model describes the process by which the itinerant electrons transit along the O^{2-}–Mn^{2+}–O^{2-}–Mn^{3+}–O^{1-} ion chains in La$_{1-x}$Sr$_x$MnO$_3$ ($x < 0.15$), wherein a $2p$ hole is present in the outer orbit of the O^{1-} anion and the magnetic moment of the Mn^{3+} cation is opposite to that of the Mn^{2+} cation.

Introduction. – The manganites $R_{1-x}T_x$MnO$_3$ with an ABO$_3$ perovskite structure, where R and T are rare-earth and alkaline-earth ions, respectively, have been studied extensively owing to their rich physics, which is related to their colossal magnetoresistance, and their potential applications in magnetic devices [1–12]. It is assumed that the spin structure and electronic transport properties of $R_{1-x}T_x$MnO$_3$ manganites are correlated via the double-exchange (DE) mechanism [13] (in which the hopping of e_g electrons between the Mn^{3+} and Mn^{4+} cations is mediated by oxygen anions). It is also believed that the antiferromagnetic spin structure of RMnO$_3$ is correlated via the magnetic superexchange (SE) interaction between the Mn^{3+} cations and is mediated by oxygen anions. However, no one has been able to explain the dependence of the observed magnetic moment, μ_{exp}, on the T doping level,

x, in the case of these manganites. This is a challenging problem that has puzzled both experimentalists and theorists for many years and was the focus of the present investigation.

In order to explain the electrical-transport properties of such ferromagnetic manganite materials (including $R_{1-x}T_x$MnO$_3$), Alexandrov *et al.* [14] proposed an O $2p$ hole model on the basis of the experimental results of a number of electron energy-loss spectroscopy (EELS), X-ray absorption spectroscopy (XAS), and nuclear magnetic resonance (NMR) studies that showed unambiguously that the current carriers are oxygen p holes and not d electrons [15–18]. The fact that p holes were observed was used to confirm the so-called current-carrier collapse (CCDC) model, which was used to describe the electrical-transport characteristics of perovskite manganites [14]. Following these reports, there have been several investigations on the electrical-transport characteristics of these

---

[(a)]E-mail: tanggd@mail.hebtu.edu.cn (corresponding author)

materials. Grenier *et al.* [19] observed the superstructures associated with the oxygen $2p$ states in two prototypical manganites through X-ray diffraction analysis at the oxygen K edge. Mizoroki *et al.* [20] carried out magnetic Compton scattering measurements on polycrystalline samples of the perovskite manganites $La_{1-x}Sr_xMnO_3$ and found that the doped holes predominantly enter the O $2p$ states in the lightly doped region. Xu *et al.* [21] modeled the temperature dependence of the electrical resistivity of perovskite manganites $Nd_{0.5}Ca_{0.5-x}Sr_xMnO_3$.

Given that p holes exist in the outer orbits of the O^{1-} ions, this suggested that O^{1-} ions are present in these oxides, in addition to O^{2-} ions. The fact that O^{1-} ions as well as O^{2-} ions are present in these oxides has further been confirmed through density functional theory (DFT) calculations and several experimental studies.

For the perovskite oxide $BaTiO_3$, Cohen *et al.* [22,23] calculated the valence electron density of states (DOS) using DFT; their results indicated that the average valences of Ba, Ti, and O are $+2$, $+2.89$, and -1.63, respectively, rather than $+2$, $+4$, and -2, as was assumed in the conventional view. These values suggest that only Ti^{2+} and Ti^{3+} cations are present in $BaTiO_3$, with Ti^{4+} cations being absent. As an approximation, if the value of the oxide ionicity, f_i, is taken to be half of the average valence of the oxygen anions, V_{alO}, $BaTiO_3$'s ionicity can be estimated to be $f_i = |V_{alO}|/2 = 0.815$. We note that this approximate result is in good qualitative agreement with the results of other ionicity studies [24–26].

Dupin *et al.* [27] proposed that some O ions in several oxides are O^{1-} ions, based on the X-ray photoelectron spectra (XPS), and calculated the average net charges of the oxygen ions, q_o. In particular, they determined that the average net charges of TiO_2, ZrO_2, CoO, CaO, and SrO are -1.15, -1.18, -1.05, -1.78, and -1.85, respectively. Here, the average net charge, q_o, can be understood as the average valence of the oxygen ions, V_{alO}. Since the conventional valence of O is considered to be -2, these reduced values also implied that O^{1-} anions must also be present in these oxides, in addition to O^{2-} anions. Moreover, the average valences of Ti and Zr in TiO_2 and ZrO_2 were determined to be $+2.30$ and $+2.36$, respectively, rather than $+4$ in the conventional view, and these values also suggest that no tetravalent cations are present in these oxides. Thus, it can be concluded that only divalent and trivalent Ti and Zr cations are present in TiO_2 and ZrO_2.

Following Dupin *et al.* in a recent work, we found that the average valences of the O ions in polycrystalline bulk samples of $BaTiO_3$ [28] and $SrTiO_3$ [29] were -1.55 and -1.62, respectively; both these values are close to that (-1.63) calculated by Cohen *et al.* for $BaTiO_3$ [22,23]. In addition, we obtained a very interesting result: the estimated ionicity, f_i (*i.e.*, half the average oxygen valency, $|V_{alO}|/2$) decreased approximately linearly with an increase in the cation second ionization energy, V_{2i} [28], which is in very close agreement to the results reported
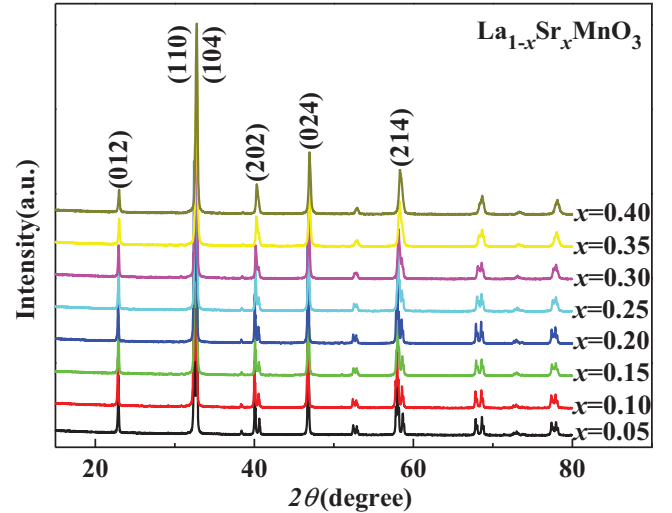

Fig. 1: (Colour online) XRD patterns of the $La_{1-x}Sr_xMnO_3$ samples.

by Phillips [24]. In similar studies, both Guo *et al.* [30] and Raddy *et al.* [31] reported the ionicities of several other dioxide materials. Based on these results, one may determine the qualitative relation $f_i < 0.75$ when the fourth ionization energy $V_{4i} > 43.5\,eV$. This relation also suggests the absence of quadrivalent cations when $V_{4i} > 43.5\,eV$. The variation in the ionicity with the ionization energy of the cations can be understood as follows: it is difficult to remove an electron with a high ionization energy from its cation. In addition, our group performed XPS analysis on two $SrTiO_3$ samples subjected to argon ion etching for different durations [29]. We found that the absolute values of the average valences of O and Ti ions in the two samples increased and decreased, respectively, with an increase in the etching time; this was due to the fact that the O/Ti ion content ratio decreased with an increase in the etching time.

Thus, given that the fourth ionization energy of a Mn cation is $51.2\,eV$, as suggested by previous studies, and by assuming that no Mn^{4+} cations were present in the $La_{1-x}Sr_xMnO_3$ ($0.05 \le x \le 0.40$) samples studied in this work, we could explain their magnetic structure and fit the dependence of their magnetic moments on the Sr doping level using an O $2p$ itinerant electron model similar to the O $2p$ hole model proposed by Alexandrov *et al.* [14].

Experiment and results. – Powder samples of $La_{1-x}Sr_xMnO_3$ with Sr contents of $0.05 \le x \le 0.40$ were prepared using the sol-gel method [32–34]. The detailed experimental procedures were as follows. First, La_2O_3 was thermally treated at $1073\,K$ for $3\,h$ to remove H_2O and CO_2. Next, stoichiometric quantities of La_2O_3, $Sr(NO_3)_2$, and $Mn(NO_3)_2$ were dissolved in a dilute HNO_3 solution, and suitable amounts of citric acid and ethylene glycol were added as complexing agents until a completely homogeneous transparent solution was obtained. This solu-
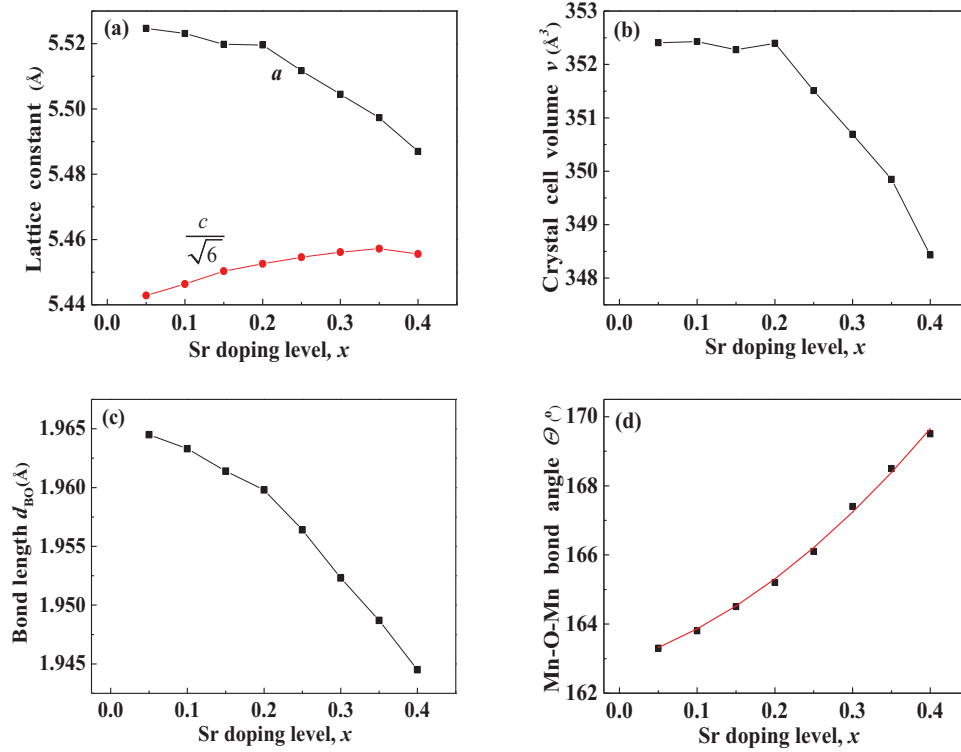
Fig. 2: (Colour online) Dependence on Sr doping level, x, of (a) lattice parameters a and c, (b) cell volume v, (c) Mn-O bond length d_{BO}, and (d) Mn–O–Mn bond angles Θ.

tion was subjected to slow evaporation at $363\,K$ in a water bath until a highly viscous gel was formed. This gel was subsequently heated at $473\,K$ for $24\,h$ until it was completely dry. Second, after grinding, the obtained powder was subjected to further heat treatment. In our heating procedure, the temperature was first increased in steps of $25\,K$ from 473 to $673\,K$, with the temperature held for $30\,min$ at each step. Following this, the temperature was further increased in steps of $10\,K$ from 673 to $773\,K$, with the temperature also held for 30 min at each step. The powder was then thermally treated at $773\,K$ for $10\,h$ before being gradually cooled during furnace cooling. At this point, the powder samples had already formed the ABO_3 perovskite structure, but owing to the small diameter of the crystallites, which affected our analysis of the intrinsic magnetism, they required further thermal treatment [10]. Thus, after the samples were calcined at $873\,K$ for $5\,h$ and $1073\,K$ for $10\,h$, in sequence, the powders were then compressed into pellets measuring $13\,mm$ in diameter and $2\,mm$ in thickness to promote contact at the grain boundaries before they were calcined for $10\,h$ at a temperature of $1273\,K$. Finally, the sample powders obtained by grinding the sintered pellets were calcined once more at a temperature of $1273\,K$ for $10\,h$ to obtain the polycrystalline powders of $La_{1-x}Sr_xMnO_3$ studied in this work. It is worth noting that each thermal treatment was performed in a muffle furnace.

X-ray powder diffraction (XRD) patterns were analysed using the *X'Pert HighScore Plus* software suite

(PANalytical), and these patterns are shown in fig. 1 for a range of Sr doping levels, x. All the samples were found to consist of a single ABO_3 perovskite phase with the space group $R\bar{3}c$, and the volume-averaged diameters of the crystallites in each sample were estimated based on the Scherrer equation. In every case, these diameters were found to be greater than or close to $100\,nm$. Thus, it was assumed that the surface effects would be very weak [10].

Next, Rietveld fittings of the XRD patterns of the samples were performed. The fitting results for the lattice parameters, a and c, the crystal cell volume, v, the B–O (Mn–O) bond length, d_{BO}, and the B–O–B (Mn–O–Mn) bond angle, θ, are shown in fig. 2. As the doping level, x, increases, a number of distinctive features are observed: i) there is a characteristic doping level, $x_1 = 0.15$, such that when $x < 0.15$, the magnitude of the Mn–O bond length, d_{BO}, changes only slightly, while it undergoes a more significant reduction with an increase in x when $x > 0.15$; ii) there is another characteristic doping level, $x_2 = 0.20$, for the lattice constant a and the crystal cell volume v, such that both a and v change only slightly when $x < 0.20$, while both of them decrease with an increase in x when $x > 0.20$; and iii) the Mn–O–Mn bond angle, θ, increases gradually with an increase in x. We would like to note that these dependences of the crystal structure parameters on the doping level, x, are related to each sample's magnetic moment, as shown below.

In order to estimate the average valences of the ions in the samples, we measured the O $1s$ photoelectron spec-
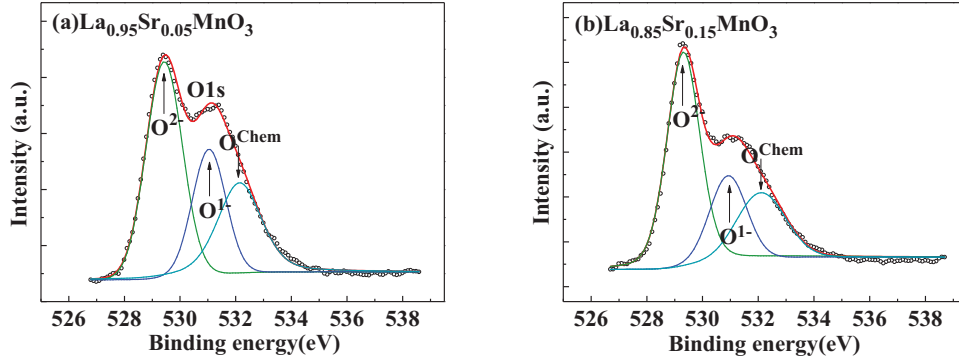
Fig. 3: (Colour online) Fitting results of O 1s XPS spectra of (a) La$_{0.95}$Sr$_{0.05}$MnO$_3$ and (b) La$_{0.85}$Sr$_{0.15}$MnO$_3$. Points and curves represent the observed and fitted results, respectively.

Table 1: Specific saturation magnetization (σ_S) values of La$_{1-x}$Sr$_x$MnO$_3$ samples measured at 10 K. μ_{exp} is the magnetic moment per formula of the samples at 10 K and T_c is the Curie temperature of the samples. Values of μ_{exp} and T_c reported by Urushibara [5] and Jonker [35] are also listed.

Sr content	σ_S (A· m^2/kg)	Magnetic moment μ_{exp} (μ_B/formula)			T_c (K)	
x	This work	This work	Urushibara [5]	Jonker [35]	This work	Urushibara [5]
0.00	–	–	–	0.00	–	–
0.05	54.45	2.33	–	–	107.7	–
0.10	77.20	3.27	3.6	3.08	168.3	145
0.15	99.91	4.19	4.2	–	216.5	238
0.20	85.15	3.53	3.9	3.73	292.7	309
0.25	84.09	3.45	3.9	–	313.7	342
0.30	83.72	3.39	3.5	3.71	337.2	369
0.35	79.95	3.21	–	3.66	350.4	–
0.40	79.88	3.17	3.4	3.51	348.9	371

tra of the samples La$_{1-x}$Sr$_x$MnO$_3$ ($x = 0.05$ and 0.15) using an XPS system (PHI5000 Versa Probe) with a monochromatic Al–K$_\alpha$ radiation (1486.6 eV) source. The C 1s binding energy (284.8 eV) of a carbon contaminant was used for calibration in order to compensate for the charging effects. The computer program XPSPEAK (Version 4.1) was used to fit the narrow-scan spectra after Shirley-type background subtraction. The narrow-scan spectra of the O 1s peaks were fitted using symmetric Gaussian-Lorentzian product functions.

Figures 3(a) and (b) show the O 1s spectra of the samples La$_{1-x}$Sr$_x$MnO$_3$ ($x = 0.05$ and 0.15). It can be seen that the O 1s spectra can be fitted using three peaks with different binding energies (BEs). According to the interpretation suggested by Dupin *et al.* [27] and Wu *et al.* [28,29], the lowest BE peak can be assigned to O^{2-} ions, the middle peak to O^{1-} ions, and the highest peak to O^{Chem}, that is, the oxygen chemically adsorbed on the surface of the sample. Setting $O_1/O_2 = S_1/S_2$, where O_1/O_2 and S_1/S_2 represent the content ratio and peak area ratio of the O^{1-} and O^{2-} anions, respectively, and requiring that $O_1 + O_2 = 1$, we get

$$O_2 = \frac{1}{1 + S_1/S_2}, \qquad O_1 = 1 - O_2. \qquad (1)$$

The average valence, V_{alO}, of the oxygen anions can be obtained as follows:

$$V_{alO} = -2O_2 - O_1. \qquad (2)$$

Thus, the V_{alO} for the samples with $x = 0.05$ and 0.15 were determined to be -1.65 and -1.77, respectively. These values are close to the average valence (-1.63) of oxygen in BaTiO$_3$ as calculated by Cohen [22,23]. Additionally, the ionicities, $f_O = |V_{alO}|/2$, of the two samples were determined to be 0.825 and 0.885, respectively. Although it is difficult to accurately measure the valences of the ions in an oxide using XPS owing to the effect of the oxygen content of the test sample [29], it could be confirmed that the absolute values of the valences of the cations and anions were lower than the conventional values.

The magnetic hysteresis of each La$_{1-x}$Sr$_x$MnO$_3$ sample was measured at 10 K. The resulting specific saturation magnetizations, σ_S, and magnetic moments, μ_{exp}, per formula are listed in table 1. The Curie temperatures, T_c, of the samples have a slight difference with those reported by Urushibara [5], as can be seen from table 1. This difference is attributed to the fact that their single crystal samples were grown by alternative means to that used in this work (*i.e.*, their samples were grown using the floating-zone (FZ) method). It can also be observed that μ_{exp}
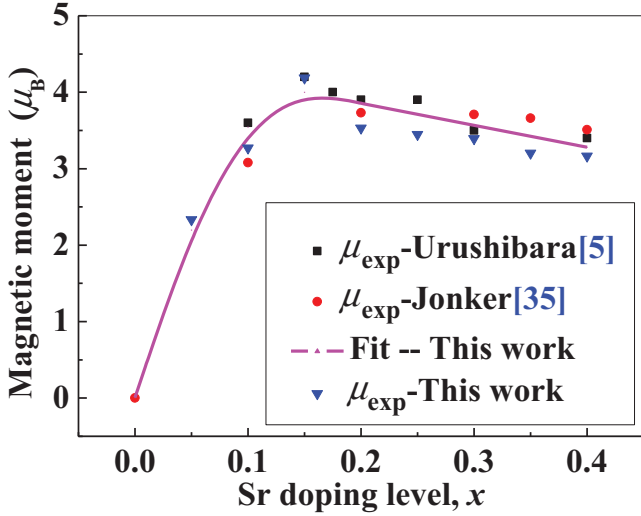
Fig. 4: (Colour online) Fitted (curve) dependence on Sr doping level, x, of magnetic moments of $La_{1-x}Sr_xMnO_3$ samples and results observed in this work ($\blacktriangledown$), as well as data reported by Urushibara ($\blacksquare$) [5], and Jonker ($\bullet$) [35].

increases rapidly with an increase in x when $x \leq 0.15$ but decreases slowly for $x \geq 0.15$. The maximum observed value, $\mu_{exp} = 4.19\mu_B$, occurs when $x = 0.15$. We would like to note that this observed trend in μ_{exp} is very similar to those reported by Urushibara [5] and Jonker [35]; these are also shown in table 1 and fig. 4 for comparison. In fig. 4, the points represent the experimental results while the curve represents the fit obtained from the analysis presented in the following section.

Discussion. – In keeping with previous reports [14–31] and the experimental results shown in fig. 3, we assumed that both O^{1-} anions and O^{2-} anions were present in the tested oxides and that there were no tetravalent Mn^{4+} cations in the samples. Therefore, an O $2p$ hole must be present in the outer orbit of the O^{1-} anions, while the O^{2-} anions must have a full outer electron shell with 8 electrons. Given the similarity of the test system to the O $2p$ hole model [14–18], we analyzed the magnetic ordering in these materials using an O $2p$ itinerant electron model for magnetic oxides (IEO model) that was recently proposed by our group [36]. We would like to mention that this IEO model has already been used to fit the dependence of the magnetic moment on the doping level for several series of spinel ferrites [37–46] and perovskite manganites [47,48].

The IEO model is based on the following three postulates [36]: i) O^{1-} anions are present in oxides and there are $2p$ holes in the outer orbits of these O^{1-} anions; ii) the two O $2p$ electrons in the outer orbit of an O^{2-} anion (which have opposite spin directions) become itinerant electrons in the two different sublattices (the A or B sites); and iii) the magnetic ordering in the B sublattice of the ABO_3 perovskite manganites $La_{1-x}Sr_xMnO_3$ is dependent on the number of $3d$ electrons, n_d (including both the local

and the itinerant $3d$ electrons of the Mn cations) and is subject to the constraints arising from Hund's rules [49].

Thus, there is a certain probability that a $2p$ electron of an O^{2-} anion can hop to a $2p$ hole in an adjacent O^{1-} anion (while maintaining a constant spin direction) in a process mediated by the valence electrons of the cations. This hopping process can, of course, also be understood as a $2p$ hole hopping in the opposite direction. Moreover, since we know that a maximum of five electrons can have their spins aligned in one direction in the $3d$ subshell of transition metal atoms, when an itinerant electron hops to a Mn^{3+} cation ($n_d = 4$), the spin direction of this itinerant electron must be parallel to the spin direction of the local $3d$ electrons (majority spins). However, when an itinerant electron hops to a Mn^{2+} cation ($n_d = 5$), the spin direction of this itinerant electron must be antiparallel to the spin direction of the local $3d$ electrons. Therefore, the directions of the magnetic moments of the Mn^{2+} cations at the B sites must be antiparallel to those of the Mn^{3+} cations, because the spin direction of the itinerant electron remains constant during the hopping process. Thus, according to the IEO model, the direction of the magnetic moment of the Mn^{2+} cations in $LaMnO_3$ is opposite to that of the magnetic moment of the Mn^{3+} cations.

As can be seen from fig. 4, Urushibara *et al.* [5] and Jonker [35] observed that the maximum magnetic moment ($\sim 4\mu_B$) occurred at doping levels of $x = 0.15$ and 0.20, respectively. According to our own experimental results, the maximum magnetic moment value was obtained at $x = 0.15$. In order to fit the observed maximum magnetic moments, we assumed that the valence of all Mn cations is $+3.0$ when $x = 0.15$. In other words, we assumed that the ionicity of the Mn cations, $f_{M0.15}$, is 1.00.

As is well known, the Mn cations in $LaMnO_3$ have an antiferromagnetic structure [1–3,5,35]. As the ratio of the magnetic moments of the Mn^{2+} and Mn^{3+} cations is $5/4$ and since the total magnetic moment of the sample is zero [35], one can readily determine that the content ratio of the Mn^{2+} and Mn^{3+} cations is $4/5$. Therefore, the ionicity of the Mn cations may be estimated from

$$f_{M0.00} = \left(2 \times \frac{4}{9} + 3 \times \frac{5}{9}\right) \Big/ 3 = 0.8519. \qquad (3)$$

where the denominator 3 is attributable to the fact that the ionicity of Mn is 1.0 when the valence of Mn in this oxide is 3.0.

Then, in order to fit the observed trend in the sample magnetic moments as a function of x when $x \leq 0.15$ (as shown in table 1 and fig. 4), we assumed that the ionicity of the Mn cations varied as

$$f_{Mx} = \sin(\theta_1 + cx) \quad (0.00 \leq x \leq 0.15).$$

By applying the conditions $f_{M0.00} = 0.8519$ and $f_{M0.15} = 1.00$, we could then easily calculate the fitting parameters and obtain a fit:

$$f_{Mx} = \sin(1.0196 + 3.6747x) \quad (0.00 \leq x \leq 0.15). \qquad (4)$$

Using eq. (4), the contents of the Mn^{2+} and Mn^{3+} cations, M_2 and M_3, could also be obtained:

$$M_2 = 3 - 3f_{Mx}, \quad M_3 = 1 - M_2 \quad (0.00 \leq x \leq 0.15), \quad (5)$$

Based on these expressions, the magnetic moment of the samples could then be obtained as follows:

$$\mu_{\mathrm{cal}} = 4M_3 - 5M_2 \quad (0.00 \leq x \leq 0.15). \quad (6)$$

In order to explain the fact that the magnetic moments decrease with an increase in x when $x > 0.15$, we assumed that the samples have a canted ferromagnetic structure and that the angle between the magnetic moments of the Mn^{3+} cations is greater than zero when $x > 0.15$. We also assumed that the magnetic moments vary linearly with x as shown below:

$$\mu_{\mathrm{cal}} = 4[1 - 0.72(x - 0.15)] \quad (0.15 \leq x \leq 0.40), \quad (7)$$

where the parameter 0.72 was obtained by fitting the model with the data presented in table 1. As was mentioned earlier, fig. 4 shows the measured and calculated dependencies of the magnetic moments of $La_{1-x}Sr_xMnO_3$ on the Sr doping level, x, where the solid curve represents the fitted result obtained using eqs. (6) and (7). The different points represent the magnetic moments observed in this work ($\blacktriangledown$), those reported by Urushibara ($\blacksquare$) [5], and those observed by Jonker ($\bullet$) [35] (see also table 1). One can see that our fitted curve is in very good agreement with the average value of the observed results. The observed magnetic moments in the three sets of samples for the same composition have slightly different values due to the different methods used to prepare the samples. The first set of samples we considered were single crystals that were grown using the FZ method by Urushibara *et al.* [5]. The second set of samples were polycrystalline powders that were prepared using a ceramic technique with a maximum thermal treatment temperature of $1450\,°C$ by Jonker *et al.* [35]. The third set of samples we considered were the polycrystalline powders studied in this work, which were prepared using the sol-gel method with a maximum thermal treatment temperature of $1000\,°C$.

Finally, the average angle ϕ between the magnetic moments of the Mn^{3+} cations could also be obtained from eq. (7) and is given by

$$\phi = \frac{180}{\pi}\arccos[1 - 0.72(x - 0.15)] \quad (0.15 \leq x \leq 0.40),$$
$$(8)$$

where the angle ϕ is expressed in degrees. A simple calculation shows that, at the highest level of doping considered, that is, at $x = 0.40$, the canting angle is significantly larger than zero, *i.e.*, $\phi = 34.9°$. We would like to note that our assumption regarding the canted magnetic structure of the Mn cations has been confirmed by magnetoresistance experiments performed on $Pr_{0.6}Sr_{0.4}MnO_3$ [47].

Conclusion. – Following the oxygen $2p$ hole model proposed by Alexandrov *et al.*, we could successfully explain the magnetic structures of the perovskite manganites $La_{1-x}Sr_xMnO_3$ using an oxygen $2p$ itinerant electron model. On the basis of previous ionicity investigations and XPS analyses, we assumed that only Mn^{2+} and Mn^{3+} cations were present in the tested samples, with tetravalent Mn^{4+} cations being absent. We found that, when the Sr doping level, x, is in the range $0.0 \leq x \leq 0.15$, the content ratio of the Mn^{2+} and Mn^{3+} cations decreases from $4/5$ ($x = 0.00$) to 0 ($x = 0.15$), resulting in the magnetic moments increasing from 0 ($x = 0.00$) to $4\mu_B$ ($x = 0.15$). This behavior is due to the magnetic moment direction of the Mn^{2+} cations being opposite to that of the Mn^{3+} cations. When $x = 0.15$, the magnetic moment of the sample reaches its maximum value and all the Mn cations are assumed to be Mn^{3+} cations. For higher Sr doping levels, *i.e.*, for $0.15 < x \leq 0.40$, the samples are assumed to have a canted ferromagnetic structure and the angle between the Mn^{3+} cation magnetic moments is assumed to be greater than zero. This increase in the canting angle causes the magnetic moment of the samples to decrease with the increase in the Sr content. The analysis reported here highlights the suitability of the IEO model in elucidating the magnetic ordering of $La_{1-x}Sr_xMnO_3$ and in fitting the dependence of the magnetic moments of the $La_{1-x}Sr_xMnO_3$ samples measured at $10\,K$ on the Sr doping level, x.

$$* * *$$

REFERENCES

[1] SALAMON MYRON B. and JAIME M., *Rev. Mod. Phys.*, **73** (2001) 583.
[2] DAGOTTO E., HOTTA T. and MOREO A., *Phys. Rep.*, **344** (2001) 1.
[3] TOKURA Y. and TOMIOKA Y., *J. Magn. & Magn. Mater.*, **200** (1999) 1.
[4] VON HELMOLT R., WECKER J., HOLZAPFEL B., SCHULTZ L. and SAMWER K., *Phys. Rev. Lett.*, **71** (1993) 2331.
[5] URUSHIBARA A., MORITOMO Y., ARIMA T., ASAMITSU A., KIDO G. and TOKURA Y., *Phys. Rev. B.*, **51** (1995) 14103.
[6] TANG G. D., HOU D. L., LI Z. Z., ZHAO X., QI W. H., LIU S. P. and ZHAO F. W., *Appl. Phys. Lett.*, **89** (2006) 261919.
[7] TANG G. D., HOU D. L., CHEN W., HAO P., LIU G. H., LIU S. P., ZHANG X. L. and XU L. Q., *Appl. Phys. Lett.*, **91** (2007) 152503.

[8] TANG G. D., LIU S. P., ZHAO X., ZHANG Y. G., JI D. H., LI Y. F., QI W. H., CHEN W. and HOU D. L., *Appl. Phys. Lett.*, **95** (2009) 121906.

[9] HONG F., CHENG Z. X., WANG J. L., WANG X. L. and DOU S. X., *Appl. Phys. Lett.*, **101** (2012) 102411.

[10] JI D. H., TANG G. D., LI Z. Z., HAN Q. J., HOU X., BIAN R. R. and LIU S. R., *J. Appl. Phys.*, **111** (2012) 113902.

[11] GOLDYREVA E. I., LEONIDOV I. A., PATRAKEEV M. V., CHUKIN A. V., LEONIDOV I. I. and KOZHEVNIKOV V. L., *J. Alloys Compd.*, **638** (2015) 44.

[12] KHAN M. H., PAL S. and BOSE S., *J. Magn. & Magn. Mater.*, **391** (2015) 140.

[13] ZENER C., *Phys. Rev.*, **82** (1951) 403.

[14] ALEXANDROV A. S., BRATKOVSKY A. M. and KABANOV V. V., *Phys. Rev. Lett.*, **96** (2006) 117003.

[15] NÜCKER N., FINK J., FUGGLE J. C., DURHAM P. J. and TEMMERMAN W. M., *Phys. Rev. B*, **37** (1988) 5158.

[16] JU H. L., SOHN H.-C. and KRISHNAN KANNAN M., *Phys. Rev. Lett.*, **79** (1997) 3230.

[17] IBRAHIM K., QIAN H. J., WU X., ABBAS M. I., WANG J. O., HONG C. H., SU R., ZHONG J., DONG Y. H., WU Z. Y., WEI L., XIAN D. C., LI Y. X., LAPEYRE G. J., MANNELLA N., FADLEY C. S. and BABA Y., *Phys. Rev. B*, **70** (2004) 224433.

[18] PAPAVASSILIOU G., PISSAS M., BELESI M., FARDIS M., KARAYANNI M., ANSERMET J. P., CARLIER D., DIMITROPOULOS C. and DOLINSEK J., *Europhys. Lett.*, **68** (2004) 453.

[19] GRENIER S., THOMAS K. J., HILL J. P., STAUB U., BODENTHIN Y., GARCÍA-FERNÁNDEZ M., SCAGNOLI V., KIRYUKHIN V., CHEONG S-W., KIM B. G. and TONNERRE J. M., *Phys. Rev. Lett.*, **99** (2007) 246403.

[20] MIZOROKI T., ITOU M., TAGUCHI Y., IWAZUMI T. and SAKURAI Y., *Appl. Phys. Lett.*, **98** (2011) 052107.

[21] XU LISHA, FAN JIYU, ZHU YAN, SHI YANGGUANG, ZHANG LEI, PI LI, ZHANG YUHENG and SHI DANING, *Chem. Phys. Lett.*, **634** (2015) 174.

[22] COHEN R. E., *Nature*, **358** (1992) 136.

[23] COHEN R. E. and KRAKAUER H., *Phys. Rev. B*, **42** (1990) 6416.

[24] PHILLIPS J. C., *Rev. Mod. Phys.*, **42** (1970) 317.

[25] THOMAS J. and POLLINI I., *Phys. Rev. B*, **32** (1985) 2522.

[26] JI D. H., TANG G. D., LI Z. Z., HOU X., HAN Q. J., QI W. H., BIAN R. R. and LIU S. R., *J. Magn. & Magn. Mater.*, **326** (2013) 197.

[27] DUPIN J. C., GONBEAU D., VINATIER P. and LEVASSEUR A., *Phys. Chem. Chem. Phys.*, **2** (2000) 1319.

[28] WU L. Q., LI Y. C., LI S. Q., LI Z. Z., TANG G. D., QI W. H., XUE L. C., GE X. S. and DING L. L., *AIP Adv.*, **5** (2015) 097210.

[29] WU L. Q., LI S. Q., LI Y. C., LI Z. Z., TANG G. D., QI W. H., XUE L. C., DING L. L. and GE X. S., *Appl. Phys. Lett.*, **108** (2016) 021905.

[30] GUO Y. Y., KUO C. K. and NICHOLSON P. S., *Solid State Ion.*, **123** (1999) 225.

[31] REDDY R. R., GOPAL K. R., NAZEER AHAMMED Y., NARASIMHULU K., SIVA SANKAR REDDY L. and KRISHNA REDDY C. V., *Solid State Ion.*, **176** (2005) 401.

[32] LIU S. P., TANG G. D., HAO P., XU L. Q., ZHANG Y. G., QI W. H., ZHAO X., HOU D. L. and CHEN W., *J. Appl. Phys.*, **105** (2009) 013905.

[33] LIU S. P., XIE Y., XIE J. and TANG G. D., *J. Appl. Phys.*, **110** (2011) 123714.

[34] LIU S. P., XIE Y., TANG G. D., LI Z. Z., JI D. H., LI Y. F. and HOU D. L., *J. Magn. & Magn. Mater.*, **324** (2012) 1992.

[35] JONKER G. H. and VAN SANTEN J. H., *Physica*, **16** (1950) 337.

[36] XU J., MA L., LI Z. Z., LANG L. L., QI W. H., TANG G. D., WU L. Q., XUE L. C. and WU G. H., *Phys. Status Solidi B*, **252** (2015) 2820.

[37] TANG G. D., HAN Q. J., XU J., JI D. H., QI W. H., LI Z. Z., SHANG Z. F. and ZHANG X. Y., *Phys. B*, **438** (2014) 91.

[38] SHANG Z. F., QI W. H., JI D. H., XU J., TANG G. D., ZHANG X. Y., LI Z. Z. and LANG L. L., *Chin. Phys. B*, **23** (2014) 107503.

[39] LANG L. L., XU J., QI W. H., LI Z. Z., TANG G. D., SHANG Z. F., ZHANG X. Y., WU L. Q. and XUE L. C., *J. Appl. Phys.*, **116** (2014) 123901.

[40] ZHANG X. Y., XU J., LI Z. Z., QI W. H., TANG G. D., SHANG Z. F., JI D. H. and LANG L. L., *Phys. B*, **446** (2014) 92.

[41] LANG L. L., XU J., LI Z. Z., QI W. H., TANG G. D., SHANG Z. F., ZHANG X. Y., WU L. Q. and XUE L. C., *Phys. B*, **462** (2015) 47.

[42] XU J., JI D. H., LI Z. Z., QI W. H., TANG G. D., ZHANG X. Y., SHANG Z. F. and LANG L. L., *Phys. Status Solidi B*, **252** (2015) 411.

[43] XU J., QI W. H., JI D. H., LI Z. Z., TANG G. D., ZHANG X. Y., SHANG Z. F. and LANG L. L., *Acta Phys. Sin.*, **64** (2015) 017501 (in Chinese with English Abstract).

[44] XUE L. C., LANG L. L., XU J., LI Z. Z., QI W. H., TANG G. D. and WU L. Q., *AIP Adv.*, **5** (2015) 097167.

[45] DING L. L., XUE L. C., LI Z. Z., LI S. Q., TANG G. D., QI W. H., WU L. Q. and GE X. S., *AIP Adv.*, **6** (2016) 105012.

[46] TANG G. D., SHANG Z. F., ZHANG X. Y., XU J., LI Z. Z., ZHEN C. M., QI W. H. and LANG L. L., *Physica B*, **463** (2015) 26.

[47] GE X. S., WU L. Q., LI S. Q., LI Z. Z., TANG G. D., QI W. H., ZHOU H. J., XUE L. C. and DING L. L., *AIP Adv.*, **7** (2017) 045302.

[48] WU L. Q., QI W. H., LI Y. C., LI S. Q., LI Z. Z., TANG G. D., XUE L. C., GE X. S. and DING L. L., *Acta Phys. Sin.*, **65** (2016) 027501 (in Chinese with English Abstract).

[49] CHEN C. W., *Magnetism and Metallurgy of Soft Magnetic Materials* (North-Holland Publishing Company) 1977, pp. 171–417.